Patterns

Federated learning for multi-omics: A performance evaluation in Parkinson's disease

Highlights

- A performance evaluation of open-source, federated learning models

- Comparison of centralized ML disease classification models against FL models

- A study of the performance of FL models trained in various federation conditions

- A validation of the results on an independent cohort

Authors

Benjamin P. Danek, Mary B. Makarious, Anant Dadu, ..., Mike A. Nalls, Jimeng Sun, Faraz Faghri

Correspondence

faraz@datatecnica.com

In brief

In this paper, the authors conduct a performance evaluation of federated machine learning algorithms for multi-omics Parkinson's disease diagnosis. The top-performing federated algorithm scores 87.6% AUC-PR on withheld data, within 2% of the top-performing central machine learning algorithm. This study revealed that federated learning can enable collaborative machine learning training on datasets siloed by policy boundaries and cloud service providers.

CellPress

Patterns

Article

Federated learning for multi-omics: A performance evaluation in Parkinson's disease

Benjamin P. Danek,[1,2,3] Mary B. Makarious,[4,5,6] Anant Dadu,[2,3] Dan Vitale,[2,3] Paul Suhwan Lee,[2] Andrew B. Singleton,[2,4] Mike A. Nalls,[2,3,4] Jimeng Sun,[1,7] and Faraz Faghri[2,3,4,8,*]

[1]Department of Computer Science, University of Illinois at Urbana-Champaign, Champaign, IL 61820, USA
[2]Center for Alzheimer's and Related Dementias (CARD), National Institute on Aging and National Institute of Neurological Disorders and Stroke, National Institutes of Health, Bethesda, MD 20892, USA
[3]DataTecnica, Washington, DC 20037, USA
[4]Laboratory of Neurogenetics, National Institute on Aging, National Institutes of Health, Bethesda, MD 20892, USA
[5]Department of Clinical and Movement Neurosciences, UCL Queen Square Institute of Neurology, London, UK
[6]UCL Movement Disorders Centre, University College London, London, UK
[7]Carle Illinois College of Medicine, University of Illinois at Urbana-Champaign, Champaign, IL 61820, USA
[8]Lead contact
*Correspondence: faraz@datatecnica.com
https://doi.org/10.1016/j.patter.2024.100945

THE BIGGER PICTURE The wide-scale application of artificial intelligence and computationally intensive analytical approaches in the biomedical and clinical domain is largely restricted by access to sufficient training data. This data scarcity exists due to the isolated nature of biomedical and clinical institutions, mandated by patient privacy policies in the health system or government legislation. Federated learning (FL), a machine learning approach that facilitates collaborative model training, is a promising strategy to address these restrictions. Therefore, understanding the limitations of cooperatively trained FL models and their performance differences from similar centrally trained models is crucial to valuing their implementation in the broader biomedical research community.

SUMMARY

While machine learning (ML) research has recently grown more in popularity, its application in the omics domain is constrained by access to sufficiently large, high-quality datasets needed to train ML models. Federated learning (FL) represents an opportunity to enable collaborative curation of such datasets among participating institutions. We compare the simulated performance of several models trained using FL against classically trained ML models on the task of multi-omics Parkinson's disease prediction. We find that FL model performance tracks centrally trained ML models, where the most performant FL model achieves an AUC-PR of 0.876 ± 0.009, 0.014 ± 0.003 less than its centrally trained variation. We also determine that the dispersion of samples within a federation plays a meaningful role in model performance. Our study implements several open-source FL frameworks and aims to highlight some of the challenges and opportunities when applying these collaborative methods in multi-omics studies.

INTRODUCTION

In recent years, machine learning (ML) algorithms have gained popularity as a possible vehicle for solving many long-standing research questions in the clinical and biomedical setting. Concretely, the adoption of sophisticated ML models can aid in tasks such as biomarker detection, disease subtyping,[1] disease identification,[2,3,4] and the development of novel medical interventions. The nascence of powerful predictive methods such as ML has enabled investigations into advanced analytics of granular patient features, such as genomics and transcriptomics,[5–7] to achieve the ultimate goal of precision medicine.

Adopting ML methods is constrained by access to high-quality datasets. In biomedical studies, curating such quality datasets is particularly difficult due to the sample collection and processing costs and the barriers associated with recruiting patients who meet a study's inclusion/exclusion criteria. The challenge of this task is exacerbated by the fact that institutions that typically collect biomedical samples cannot easily share human specimens' data due to data privacy regulations, such as the Health Insurance Portability and Accountability Act (HIPAA), the European Union General Data Protection Regulation (EU-GDPR), India's Personal Data Protection Act (PDPA), and Canada's Personal Information Protection and Electronic Documents Act
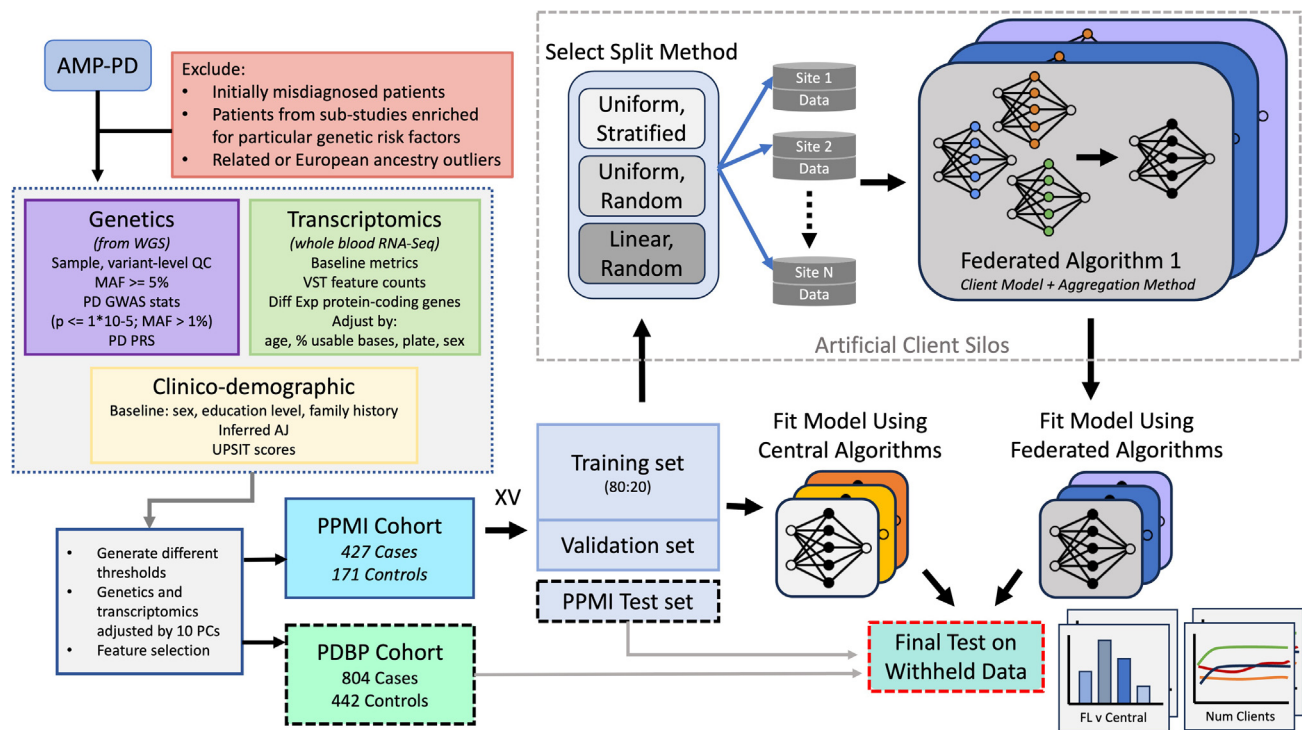
Figure 1. Experiment workflow diagram and data summary

The harmonized and joint-called PPMI and PDBP cohorts originate from the AMP-PD initiative. The PPMI cohort is split into *K* folds, where one fold is left as a holdout (internal) test set and the remaining are used for model fitting. The training folds are split using an 80:20 ratio to form the training validation split. The training split is distributed among n clients using one of the split strategies to simulate the cross-silo collaborative training setting. FL methods consist of a local learner and an aggregation method. Similarly, several central algorithms are used to fit the training data. The resultant global FL models and the ML models resulting from central training are tested on the PPMI holdout fold (internal test) and the whole PDBP test set (external test).

(IPEDA), mandated by medical systems or at a national and international level.[8]

Federated learning (FL) is an optimization method for performing ML model training among a group of clients, allowing each client to maintain governance of their local data. Initially developed for learning user behavior patterns on personal mobile devices without breaching individual privacy,[9] FL has found valuable applications in numerous domains, including finance,[10] medicine,[11,12] and the pharmaceutical industry.[13] In biomedical research, FL represents an opportunity to enable cross-silo analytics and more productive collaboration.[14–16]

This work evaluates FL methods' practical availability and utility to enable large-scale, multi-institutional and private analytics of multiple-modality biomedical samples. Specifically, we aim to identify the frameworks biomedical researchers can use to perform FL in their work, the expected performance changes, and the implementation challenges they may face. We also discuss the opportunities and limitations of applying FL in multi-omics, where samples capture a patient's genomic and transcriptomic features and clinical and demographic information through the case study of Parkinson's disease prediction.

We use the multi-modal Parkinson's disease prediction as a case study for testing FL on omics data. Timely and accurate diagnosis of neurodegenerative diseases such as Parkinson's is crucial in exploring the efficacy of novel therapies to treat and manage the disease. Since the onset of these diseases typically begins many years before any visible symptoms, early

detection is difficult to achieve at a clinical level alone. Usually it requires information inherent to the patient's biology. Makarious et al.[6] have already determined that leveraging genomic and transcriptomic information as part of the diagnosis process allows for higher model performance. This study demonstrates the feasibility and practicality of deploying FL for Parkinson's disease prediction.

RESULTS

FL models trained using publicly available and accessible framework results follow central model performance

We aim to evaluate the performance differences between classical ML algorithms frequently used in the biomedical setting against FL algorithms suitable for cross-silo modeling. An overview of our approach (Figure 1) shows the experimental design for evaluating several FL and central ML methods in the task of Parkinson's disease prediction based on genomic, transcriptomic, and clinico-demographic features (Table S1). The datasets used in experiments originate from studies providing clinical, demographic, and biological information of Parkinson's disease patients, the Parkinson's Progression Marker Initiative (PPMI) and the Parkinson's Disease Biomarkers Program (PDBP). The PPMI dataset is a longitudinal, observational study where patients contribute clinical, demographic, and imaging data as well as biological samples for whole-genome sequencing and
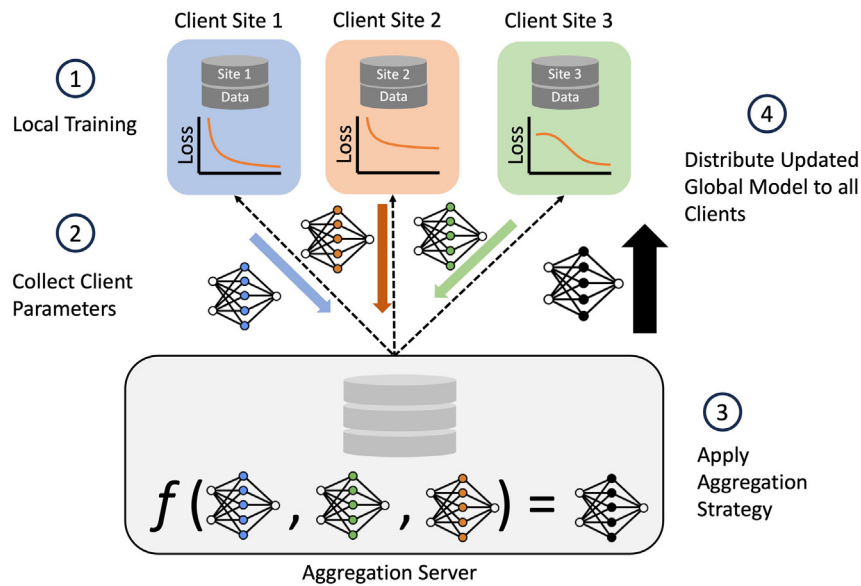
Figure 2. Federated architecture and training summary
The FL architecture used in the study also illustrates one round of FL training for the case of n = 3 clients. The aggregation server aggregates trained local learner parameters from clients and computing a global model. Client sites contain their own siloed dataset, each with different samples. The trained client parameters are represented by the blue, orange, and green weights; the black weights represent the aggregated global model. Client model aggregation implemented by the FL strategy is denoted by *f*. Once global weights are computed, a copy is sent to each client; the global model is used to initialize the local learner model weights in subsequent FL training rounds.

whole-blood RNA sequencing. PPMI specifically includes newly diagnosed and drug-naive patients, collected at clinical sites globally over a span of 5–13 years. The PDBP dataset provides clinical, genetic, imaging, and biomarker data associated with Parkinson's disease, Lewy body dementia, and other parkinsonisms. Patients in PDBP are not necessarily newly diagnosed or drug naive. The PPMI dataset is used for model training, validation, and testing. The PDBP dataset is used strictly as an external test set. In our experiments, the PPMI dataset is split into *K* folds, one of which is used as a holdout test set, with the remaining folds being used for model training and validation. To establish a baseline performance of classically trained central algorithms representative of methods used in the current biomedical research paradigm, several central ML algorithms are fit to the training set (Table S2) and tested on the holdout PPMI fold, as well as the whole PDBP dataset. To simulate the cross-silo federated setting, the training set is split into n disjoint subsets, referred to as client datasets. Where each baseline ML algorithm is fit to the full centralized training dataset, the FL model is fit to n disjoint, siloed client datasets, the union of which equates to the entire training dataset. An illustration of the FL training process is shown in Figure 2. The fitted FL models are finally evaluated against the PPMI test fold and the PDBP dataset.

In the optimistic FL setting where we compare a federation of n = 2 client sites, which have been assigned samples through uniform stratified random sampling without replacement, against the central baseline algorithms (Figure 3), it can be seen that for all the included FL methods, the absolute difference in performance is relatively small. For the internal test set, the central logistic regression (LR) classifier[17] has an area under the precision-recall curve (AUC-PR) of 0.915 ± 0.039 (standard deviation across *K* = 6 folds). Among the classifiers trained using FL, which implement the same local learner, FedAvg[18] LR, FedProx[19] μ = 0.5 LR, and FedProx μ = 2 LR, have an AUC-PR of 0.874 ± 0.042, 0.887 ± 0.041, and 0.906 ± 0.04, respectively. In the external test set, a similar relationship between central LR and federated LR is exhibited, where classical LR has an AUC-PR of 0.842 ± 0.009 and FedAvg, FedProx LR μ = 0.5 LR, and

FedProx μ = 2 LR have an AUC-PR of 0.826 ± 0.011, 0.823 ± 0.015, and 0.835 ± 0.007, respectively. This general reduction in performance between the centrally trained classifier and the classifier trained collaboratively through FL is a trend observed in nearly all of the FL algorithms across both test sets. Similarly, the central MLP classifier[20] has an AUC-PR of 0.892 ± 0.032 and 0.826 ± 0.007, respectively, while the best-performing FL variation, FedProx MLP μ = 2, has an AUC-PR of 0.868 ± 0.06 and 0.785 ± 0.015 for the internal and external test set, respectively. A similar trend can be observed for FedAvg XGBRF,[21] where the performance reduction is proportional to that observed in other learners. The only exception to this pattern is in the case of the SGD classifier,[22,23] which in the PDBP exhibits a marginal improvement of 0.002 AUC-PR. The resulting performance details, including several additional centrally trained ML algorithms, are presented in Tables 1 and 2. The statistical significance of pairwise observed differences in performance is presented in Table S3. The results of this side-by-side comparison of FL methods in an idealistic setting with minimal heterogeneity among client datasets show a relatively small difference in performance compared to the central algorithms.

Sample dispersion among client sites negatively impacts global model performance

By splitting the training samples among an increasing number of clients, we aim to understand the implications of federation configurations that have more dispersed samples (Figure 4). In both the PPMI and PDBP datasets, there is a similar relative change in AUC-PR performance when increasing the number of client sites; the absolute performance scores and variance are considerably higher for the PPMI test set than the PDBP test set. The performance of PPMI FedAvg XGBRF starts at 0.924 ± 0.015 AUC-PR in a federation of two client sites, and progressively drops to 0.861 ± 0.043 AUC-PR at 18 clients. For the PDBP performance, FedAvg XGBRF similarly reduces from 0.876 ± 0.009 to 0.752 ± 0.054 AUC-PR, at a minimum. Such a reduction in performance is also observed in the FedAvg SGD classifier, which has an AUC-PR of 0.92 ± 0.025 for two clients and an AUC-PR of 0.886 ± 0.055 for 18 clients in PPMI. In PDBP the same classifier starts at 0.847 ± 0.008 for two client sites, and ends at
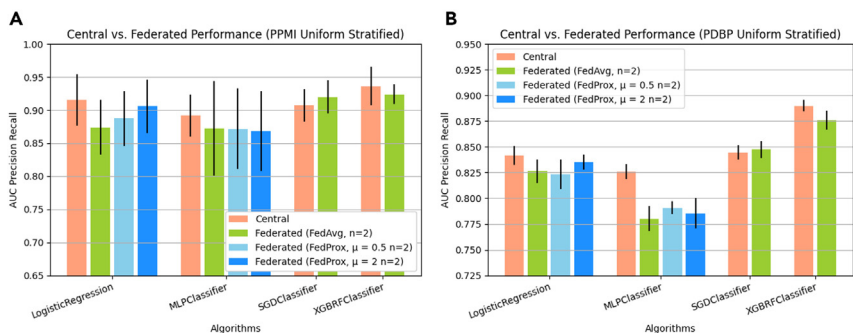
0.798 ± 0.014 AUC-PR for 18 client sites. The trend of performance decline is observed for the LR classifiers as well for both the PPMI and PDBP test sets. The FedAvg MLP, as well as both FedProx MLP classifiers, do not exhibit such a reduction performance. In the PPMI test set, FedAvg MLP performance at n = 2 client sites is 0.872 ± 0.072 AUC-PR, and at n = 18 client sites 0.876 ± 0.06. Similarly, for PDBP performance FedAvg MLP performance is 0.78 ± 0.012 for two client sites and 0.781 ± 0.009 for n = 18 client sites. A nearly identical trend is observed in FedProx μ = 0.5 and μ = 2 across both test sets. Detailed results are given in supplemental information and Tables 3 and 4.

Data heterogeneity at client sites does not significantly influence model performance

To understand the implications of data heterogeneity among client sites, we examine the change in AUC-PR in a federation of two clients with respect to the split method (Figure 5). In our experiments, we find that the performance changes introduced by dataset heterogeneity vary. Some FL models, such as FedAvg LR, FedProx μ = 0.5, FedAvg MLP, FedProx μ = 0.5 MLP, and FedProx μ = 2 MLP exhibit performance improvements as both label heterogeneity and dataset size heterogeneity are introduced. The greatest performance improvement in PDBP is 0.018 AUC-PR by FedProx μ = 2 MLP, and 0.029 by FedAvg LR in PPMI. Conversely, we find that FedProx μ = 0.5 LR, FedProx μ = 2 LR, FedAvg SGD, and FedAvg XGBRF exhibit performance degradation on account of dataset heterogeneity, where the greatest reduction in performance is 0.014 AUC-PR by XGBRF in PDBP, and 0.031 AUC-PR by FedProx μ = 2 LR in PPMI. In all such cases, the performance changes induced by dataset heterogeneity are marginal relative to other parameters such as algorithm choice or quantity of participating clients. The implications of performance heterogeneity as the number of clients increases are shown in Figures S1 and S2.

FL training time is not dramatically affected by choice in federated aggregation strategy

To shed light on the computational costs associated with using different FL aggregation strategies, we measure the model training time for FL algorithms in which the federation consists of n = 2 client sites. For the FedAvg aggregation strategy, FedAvg LR had the lowest mean runtime of 7.909e+00 ± 0.550 s. Similarly, for the algorithms implementing FedProx aggregation, FedProx μ = 0.5 LRClassifier had the lowest overall runtime of 8.747e+00 ± 0.158 s. FedProx μ = 2 LRClassifier had the sec-

ond lowest runtime for FedProx variants with a runtime of 8.905e+00 ± 0.130 s. For the MLP classifier, FedAvg, FedProx μ = 0.5, and FedProx μ = 2 had a progressively increasing runtimes 8.755e+00 ± 0.141 s, 9.039e+00 ± 0.266 s, 9.260e+00 ± 0.163 s, respectively. FedAvg XGBRF and FedAvg SGD had a considerably higher runtime of 1.061e+01 ± 0.014 and 1.513e+01 ± 1.497 s, respectively. A visualization of the runtimes for FL algorithms is presented in Figure 6.

In contrast to the FL algorithms, central algorithm training time is at least an order of magnitude lower. The fastest model to train, SGD classifier, fits the model in 6.771e−03 ± 0.001 s, and the slowest model, MLP classifier, fits its model in 1.609e−01 ± 0.009. Central LR classifier and XGBRF run in 1.857e−02 ± 0.008 and 1.633e−01 ± 0.003 s, respectively. The full list of runtimes including central and federated algorithms is presented in Table 5.

DISCUSSION

In conjunction with increased access to genomic and transcriptomic data, the proliferation of high-quality ML open-source packages has helped advance numerous long-standing challenges in biomedical research, such as disease subtyping, biomarker identification, and early disease diagnosis. The common bottleneck limiting such advances has thus shifted from the ability to apply ML methods to the availability of high-quality well-designed datasets. FL has been cited as a promising means of alleviating the data scarcity problem through data-private collaborative model training.[24–26] Previous works focus on applying FL to domains adjacent to multi-omics disease diagnosis, namely focusing on imaging data,[14,27] longitudinal health records,[15] and named entity recognition.[28] Similar works such as Salmeron et al.[29] approach benchmarking FL models on biomedical datasets but focus on comparing different FL aggregation strategies rather than evaluating FL against a central baseline, as is done in our study. By approaching FL for multi-omics disease diagnosis from a performance benchmarking perspective, focusing on algorithms that are broadly accessible in the open-source community, we hope to shed light on what kind of practical performance can be achieved in a real-world setting where deep AI and software systems expertise may be limited. We additionally aim to understand which fundamental pitfalls researchers must be aware of before applying such methods in their multi-omics tasks.

When comparing centrally trained models against collaboratively trained models that implement the same local learner algorithm, our results indicate the FL trained model performance tends to be consistently less than that of the central method

Table 1. Performance of several models trained using classical machine learning methods and federated learning methods, where the number of participating clients in the federation is n = 2, tested on the PPMI dataset

Algorithm name	ROC-AUC	AUC-PR	Balanced accuracy	Precision	Recall	F 0.5	F 1	F 2	Log loss	Matthews correlation coefficient
AdaBoost classifier	0.865 ± 0.033	0.939 ± 0.01	0.736 ± 0.069	0.844 ± 0.043	0.89 ± 0.047	0.897 ± 0.017	0.885 ± 0.027	0.942 ± 0.013	0.632 ± 0.007	0.499 ± 0.122
Bagging classifier	0.82 ± 0.05	0.916 ± 0.025	0.69 ± 0.052	0.813 ± 0.027	0.897 ± 0.061	0.865 ± 0.021	0.862 ± 0.024	0.933 ± 0.01	1.001 ± 0.382	0.428 ± 0.123
GradientBoosting classifier	0.879 ± 0.046	0.943 ± 0.026	0.723 ± 0.072	0.833 ± 0.042	0.911 ± 0.021	0.916 ± 0.03*	0.894 ± 0.022	0.942 ± 0.015*	0.444 ± 0.099	0.486 ± 0.119
KNeighbors classifier	0.61 ± 0.099	0.806 ± 0.065	0.533 ± 0.029	0.729 ± 0.014	0.937 ± 0.046	0.782 ± 0.023	0.837 ± 0.007	0.927 ± 0.004	2.836 ± 0.617	0.111 ± 0.104
LinearDiscriminantAnalysis classifier	0.763 ± 0.045	0.883 ± 0.031	0.681 ± 0.053	0.826 ± 0.04	0.77 ± 0.05	0.7 ± 0.344	0.714 ± 0.35	0.776 ± 0.38	1.608 ± 0.488	0.347 ± 0.095
LogisticRegression classifier	0.831 ± 0.068	0.915 ± 0.039	0.734 ± 0.072	0.841 ± 0.043	0.894 ± 0.028	0.872 ± 0.047	0.883 ± 0.033	0.939 ± 0.011	0.648 ± 0.203	0.493 ± 0.134
MLP classifier	0.739 ± 0.078	0.892 ± 0.032	0.703 ± 0.059	0.833 ± 0.038	0.815 ± 0.054	0.843 ± 0.038	0.858 ± 0.034	0.932 ± 0.013	6.616 ± 1.844	0.402 ± 0.119
QuadraticDiscriminantAnalysis classifier	0.504 ± 0.057	0.774 ± 0.029	0.504 ± 0.057	0.725 ± 0.055	0.385 ± 0.081	0.757 ± 0.008	0.833 ± 0.006	0.926 ± 0.003	19.674 ± 1.492	0.009 ± 0.105
RandomForest	0.816 ± 0.076	0.917 ± 0.027	0.552 ± 0.034	0.736 ± 0.016	0.993 ± 0.017*	0.857 ± 0.043	0.874 ± 0.032	0.942 ± 0.014	0.508 ± 0.029	0.249 ± 0.121
SGD classifier	0.755 ± 0.065	0.907 ± 0.025	0.735 ± 0.062	0.846 ± 0.032	0.857 ± 0.068	0.857 ± 0.037	0.876 ± 0.036	0.936 ± 0.015	7.525 ± 2.282	0.481 ± 0.143
SVC classifier	0.838 ± 0.069	0.924 ± 0.032	0.711 ± 0.071	0.827 ± 0.041	0.883 ± 0.042	0.872 ± 0.042	0.886 ± 0.024	0.941 ± 0.008	0.44 ± 0.082*	0.447 ± 0.145
XGBoost classifier	0.89 ± 0.046*	0.953 ± 0.018*	0.765 ± 0.097	0.86 ± 0.062	0.911 ± 0.03	0.915 ± 0.03	0.900 ± 0.033*	0.942 ± 0.014	0.461 ± 0.135	0.557 ± 0.167
XGBoost random forest classifier	0.857 ± 0.064	0.936 ± 0.029	0.773 ± 0.057*	0.868 ± 0.04*	0.885 ± 0.047	0.907 ± 0.039	0.891 ± 0.041	0.936 ± 0.011	1.79 ± 0.853	0.558 ± 0.105*
FedAvg LR	0.69 ± 0.16	0.874 ± 0.042	0.617 ± 0.109	0.772 ± 0.054	0.955 ± 0.037*	0.818 ± 0.054	0.863 ± 0.026	0.935 ± 0.008	0.655 ± 0.14	0.278 ± 0.25
FedAvg MLP	0.76 ± 0.102	0.872 ± 0.072	0.671 ± 0.087	0.817 ± 0.051	0.768 ± 0.089	0.708 ± 0.35	0.728 ± 0.358	0.779 ± 0.382	0.767 ± 0.308	0.334 ± 0.179
FedAvg SGD	0.828 ± 0.048	0.92 ± 0.025	0.757 ± 0.048*	0.904 ± 0.049*	0.707 ± 0.033	0.871 ± 0.032	0.872 ± 0.018	0.939 ± 0.008	0.545 ± 0.032*	0.47 ± 0.084
FedAvg XGBRF	0.829 ± 0.023*	0.924 ± 0.015*	0.739 ± 0.058	0.848 ± 0.043	0.883 ± 0.036	0.886 ± 0.02*	0.875 ± 0.012	0.929 ± 0.005	0.691 ± 0.0	0.497 ± 0.089*
FedProx μ = 0.5 LR	0.755 ± 0.142	0.887 ± 0.041	0.653 ± 0.088	0.791 ± 0.042	0.941 ± 0.031	0.704 ± 0.349	0.729 ± 0.358	0.784 ± 0.384	0.609 ± 0.155	0.362 ± 0.198
FedProx μ = 0.5 MLP	0.757 ± 0.096	0.872 ± 0.061	0.695 ± 0.088	0.829 ± 0.048	0.808 ± 0.075	0.843 ± 0.042	0.868 ± 0.028	0.937 ± 0.004	0.976 ± 0.314	0.387 ± 0.182
FedProx μ = 2 LR	0.812 ± 0.079	0.906 ± 0.04	0.658 ± 0.028	0.79 ± 0.014	0.937 ± 0.025	0.866 ± 0.045	0.879 ± 0.025*	0.941 ± 0.006*	0.582 ± 0.137	0.398 ± 0.069
FedProx μ = 2 MLP	0.765 ± 0.079	0.868 ± 0.06	0.694 ± 0.069	0.83 ± 0.042	0.798 ± 0.045	0.706 ± 0.348	0.724 ± 0.355	0.781 ± 0.382	0.9 ± 0.368	0.379 ± 0.133

Data reported are mean and standard deviation across K = 6-fold cross-validation. Best performing algorithms for each metric are indicated by an asterisk.

Table 2. Performance of several models trained using classical machine learning methods and federated learning methods, where the number of participating clients in the federation is n = 2, tested on the PDBP dataset

Algorithm name	ROC-AUC	AUC-PR	Balanced accuracy	Precision	Recall	F 0.5	F 1	F 2	Log loss	Matthews correlation coefficient
AdaBoost classifier	0.834 ± 0.021	0.891 ± 0.015	0.697 ± 0.026	0.757 ± 0.023	0.917 ± 0.033	0.835 ± 0.016	0.834 ± 0.009	0.905 ± 0.004	0.639 ± 0.005	0.456 ± 0.029
Bagging	0.812 ± 0.01	0.871 ± 0.01	0.696 ± 0.019	0.753 ± 0.015	0.932 ± 0.015	0.828 ± 0.007	0.84 ± 0.004	0.903 ± 0.003	1.291 ± 0.226	0.463 ± 0.027
GradientBoosting classifier	0.856 ± 0.013	0.9 ± 0.016	0.716 ± 0.018	0.766 ± 0.014	0.938 ± 0.013	0.856 ± 0.007	0.857 ± 0.003*	0.908 ± 0.003*	0.572 ± 0.042*	0.502 ± 0.024
KNeighbors classifier	0.586 ± 0.024	0.735 ± 0.019	0.551 ± 0.019	0.664 ± 0.011	0.946 ± 0.024	0.707 ± 0.008	0.783 ± 0.001	0.899 ± 0.0	3.322 ± 0.641	0.169 ± 0.042
LinearDiscriminantAnalysis classifier	0.702 ± 0.012	0.794 ± 0.008	0.64 ± 0.013	0.734 ± 0.01	0.776 ± 0.01	0.622 ± 0.305	0.661 ± 0.324	0.751 ± 0.368	2.104 ± 0.19	0.288 ± 0.024
LogisticRegression classifier	0.771 ± 0.011	0.842 ± 0.009	0.657 ± 0.008	0.73 ± 0.005	0.901 ± 0.01	0.791 ± 0.004	0.81 ± 0.005	0.901 ± 0.001	0.996 ± 0.039	0.368 ± 0.02
MLP classifier	0.671 ± 0.013	0.826 ± 0.007	0.619 ± 0.012	0.711 ± 0.008	0.839 ± 0.01	0.749 ± 0.009	0.789 ± 0.007	0.899 ± 0.001	8.313 ± 0.708	0.265 ± 0.026
QuadraticDiscriminantAnalysis classifier	0.525 ± 0.022	0.721 ± 0.022	0.525 ± 0.022	0.671 ± 0.024	0.366 ± 0.097	0.688 ± 0.0	0.779 ± 0.0	0.898 ± 0.0	18.716 ± 1.33	0.05 ± 0.042
RandomForest	0.736 ± 0.006	0.825 ± 0.005	0.524 ± 0.005	0.649 ± 0.003	0.985 ± 0.005*	0.764 ± 0.007	0.792 ± 0.005	0.899 ± 0.0	0.596 ± 0.004	0.132 ± 0.025
SGD classifier	0.662 ± 0.017	0.845 ± 0.007	0.65 ± 0.016	0.728 ± 0.011	0.878 ± 0.024	0.758 ± 0.01	0.803 ± 0.007	0.898 ± 0.0	10.11 ± 0.525	0.343 ± 0.034
SVC classifier	0.701 ± 0.007	0.808 ± 0.004	0.593 ± 0.011	0.693 ± 0.006	0.844 ± 0.02	0.742 ± 0.004	0.793 ± 0.002	0.901 ± 0.001	0.65 ± 0.019	0.214 ± 0.029
XGBoost classifier	0.862 ± 0.008*	0.905 ± 0.007*	0.719 ± 0.021	0.77 ± 0.016	0.932 ± 0.013	0.864 ± 0.006*	0.857 ± 0.003*	0.906 ± 0.003	0.691 ± 0.031	0.504 ± 0.03
XGBoost Random Forest classifier	0.829 ± 0.007	0.89 ± 0.006	0.732 ± 0.02*	0.781 ± 0.016*	0.918 ± 0.01	0.849 ± 0.003	0.855 ± 0.002	0.905 ± 0.003	2.715 ± 0.254	0.515 ± 0.031*
FedAvg LR	0.665 ± 0.128	0.826 ± 0.011	0.565 ± 0.052	0.673 ± 0.028	0.96 ± 0.032*	0.745 ± 0.045	0.794 ± 0.012	0.899 ± 0.002	0.829 ± 0.108	0.187 ± 0.147
FedAvg MLP	0.69 ± 0.018	0.78 ± 0.012	0.629 ± 0.01	0.719 ± 0.007	0.828 ± 0.022	0.744 ± 0.008	0.791 ± 0.007	0.899 ± 0.001	1.038 ± 0.239	0.282 ± 0.024
FedAvg SGD	0.775 ± 0.011	0.847 ± 0.008	0.689 ± 0.011	0.77 ± 0.008*	0.8 ± 0.01	0.794 ± 0.005	0.809 ± 0.004	0.902 ± 0.002	0.559 ± 0.013*	0.385 ± 0.023
FedAvg XGBRF	0.794 ± 0.007*	0.876 ± 0.009*	0.695 ± 0.023*	0.754 ± 0.017	0.919 ± 0.012	0.825 ± 0.007*	0.838 ± 0.008*	0.902 ± 0.003*	0.691 ± 0.0	0.451 ± 0.035*
FedProx μ = 0.5 LR	0.704 ± 0.101	0.823 ± 0.015	0.584 ± 0.042	0.683 ± 0.022	0.943 ± 0.03	0.762 ± 0.038	0.795 ± 0.009	0.9 ± 0.002	0.866 ± 0.092	0.232 ± 0.115
FedProx μ = 0.5 MLP	0.7 ± 0.008	0.791 ± 0.006	0.63 ± 0.011	0.719 ± 0.007	0.833 ± 0.016	0.748 ± 0.007	0.794 ± 0.004	0.899 ± 0.001	1.312 ± 0.124	0.284 ± 0.023
FedProx μ = 2 LR	0.761 ± 0.008	0.835 ± 0.007	0.601 ± 0.005	0.691 ± 0.003	0.947 ± 0.013	0.787 ± 0.008	0.804 ± 0.003	0.9 ± 0.001	0.875 ± 0.014	0.293 ± 0.01
FedProx μ = 2 MLP	0.695 ± 0.022	0.785 ± 0.015	0.631 ± 0.02	0.722 ± 0.013	0.818 ± 0.02	0.747 ± 0.014	0.791 ± 0.005	0.899 ± 0.001	1.231 ± 0.285	0.282 ± 0.044

Data reported are mean and standard deviation across K = 6-fold cross-validation. Best performing algorithms for each metric are indicated by an asterisk.
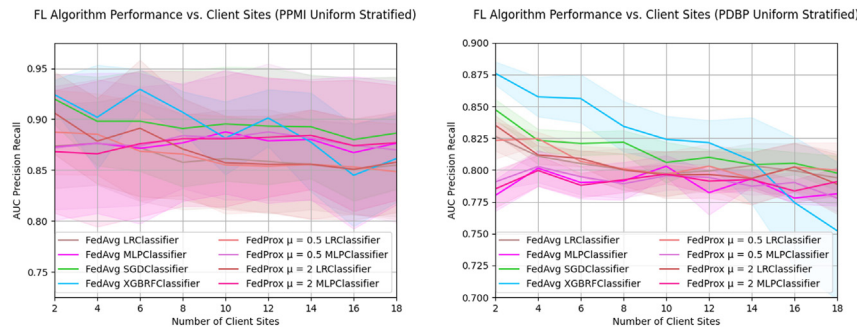
Figure 4. Sample dispersion among client sites negatively impacts global model performance

For a fixed training dataset, the AUC-PR of federated algorithms as the quantity of client sites increases. Training data are split uniformly among each member of the federation using stratified random sampling. The PDBP and PPMI datasets are used for external and internal validation, respectively. Presented data are mean score and standard deviation resulting from cross-validation.

while approximately following the performance of the central ML method. The general reduction in AUC-PR testing score between the FL and central method is noteworthy, but not a substantial deterioration. It can also be observed that for the studied aggregation strategies, FL model performance follows central model performance. In cases where the central model is performant, the FL trained model will be as well. In the case of the strongest central classifier in the central setting, XGBRF, the FL method implementing the same algorithm as a local learner, FedAvg XGBRF, also had the highest performance among models trained using FL. Additionally, we see that in many cases, FedAvg XGBRF outperforms central ML classifiers such as LR, SGD, and MLP at the same task by a significant margin. This empirical result indicates that in cases where institutions must decide between applying FL methods to their setting or centralizing data by complying with potentially stringent regulations, FL can be considered an effective option. In addition, because the implementation of such methods is available through open-source, strongly documented frameworks, the resource investment to achieve scientifically meaningful results may not be significant. We also note that because an FL model's performance tracks, and seldom exceeds, its central model performance, it can be crudely used to approximate the central model lower bound. Such an estimate of central performance, even if inexact, may be valuable for institutional stakeholders when deciding whether financial and administrative resources should be allocated to centralize several siloed datasets. We also note that the overall reduction in performance between models trained using FL methods and models trained using central methods can be attributed to the federated aggregation process, which, in our case, is implemented as the unweighted average of the local learner model weights. Such a naive averaging process detracts from the parameter optimization implemented by local learners but is a necessary cost to enable sample-private federated training. Furthermore, we note that several novel methods that implement more sophisticated weight aggregation strategies have been developed in academic settings but are not always available as generally applicable open-source packages. Overall, this test indicates that FL may be used to enable productive collaboration among institutions existing on opposite sides of geographic and policy boundaries, such as EU-GDPR, as well as across cloud providers and bare-metal servers.

In the second arm of our study, we aim to understand the model performance cost of conducting collaborative training among a federation with increasing sample dispersion. Such a situation may arise, when institutional stakeholders must comply with several layers of regulatory requirements, where centralizing some sites is easier than others. A concrete example of such a regulation is in the case of EU-GDPR, where transport of patient samples beyond the boundaries of the EU requires compliance with GDPR, and each country's respective legislation mandates the transport of samples between countries within the EU. In this series of experiments, we assume that the globally available set of samples is constant but the quantity of federation members containing the samples varies. Our experiments show that some methods, such as the LR classifiers, FedAvg SGD and FedAvg XGBRF, tend to exhibit performance degradation when there are more silos with fewer samples per silo. We also observe that methods implementing MLP as a local learner tend not to exhibit performance degradation with respect to sample concentration at silos. Such methods do not necessarily achieve the best performance for any federation configurations; however, in the most extreme federation configuration of 18 clients they are still outperformed by methods such as FedAvg SGD and FedAvg LR. Methods whose performance is not strongly affected by silo size may represent practical starting points for the application of FL in an exploratory task. Ultimately, because FL models appear to have an optimal operating point modulated by the federation configuration, the final choice in FL methods used to reach peak performance should be determined by an exhaustive search. This finding suggests that a practical future format for applying FL in the biomedical setting may be through the auto-ML paradigm, frameworks of which such as H2O[30] and Auto Sklearn[31] are currently implemented in the classical ML setting.

We additionally find in our studies that the implementation of heterogeneous client sites, with respect to dataset size and label counts, does not necessarily result in performance reductions for all algorithms. Some models such as FedAvg LR, models implementing MLP as a local learner tend to increase performance, while models such FedAvg XGBRF and FedAvg SGD exhibit performance degradation when the number of client sites is two (Figure S1). We further find that when the number of clients is four, such heterogeneity has varying effects on performance, different from the configuration with two client sites. Overall, performance changes with respect to client dataset heterogeneity are marginal relative to changes introduced by factors such number of clients per federation or algorithm selection.

When comparing training time among FL algorithms, we found a mild progression in training time between FedAvg LRClassifier, FedProx μ = 0.5 LRClassifier, and FedProx μ = 2 LR classifiers, respectively. The same trend can be observed for the FL

Table 3. AUC-PR score of models trained using federated learning as the quantity of client sites increased, tested on the PPMI dataset

		Number of clients								
		2	4	6	8	10	12	14	16	18
Algorithm name	FedAvg LR	0.874 ± 0.042	0.876 ± 0.041	0.872 ± 0.053	0.858 ± 0.046	0.861 ± 0.048	0.859 ± 0.051	0.855 ± 0.044	0.851 ± 0.045	0.855 ± 0.05
	FedAvg MLP	0.872 ± 0.072	0.876 ± 0.069	0.871 ± 0.074	0.877 ± 0.057	0.888 ± 0.061	0.879 ± 0.061	0.88 ± 0.059	0.867 ± 0.075	0.876 ± 0.06
	FedAvg SGD	0.92 ± 0.025	0.898 ± 0.044	0.898 ± 0.049	0.891 ± 0.057	0.895 ± 0.056*	0.893 ± 0.057	0.893 ± 0.051*	0.88 ± 0.06*	0.886 ± 0.055*
	FedAvg XGBRF	0.924 ± 0.015*	0.902 ± 0.051*	0.929 ± 0.02*	0.907 ± 0.02*	0.882 ± 0.036	0.901 ± 0.028*	0.878 ± 0.048	0.845 ± 0.05	0.861 ± 0.043
	FedProx μ = 0 LR	0.887 ± 0.041	0.885 ± 0.04	0.869 ± 0.048	0.866 ± 0.04	0.855 ± 0.048	0.854 ± 0.045	0.856 ± 0.054	0.853 ± 0.046	0.849 ± 0.047
	FedProx μ = 0 MLP	0.872 ± 0.061	0.876 ± 0.063	0.874 ± 0.058	0.884 ± 0.052	0.882 ± 0.061	0.888 ± 0.067	0.882 ± 0.061	0.874 ± 0.067	0.87 ± 0.071
	FedProx μ = 2 LR	0.906 ± 0.04	0.879 ± 0.042	0.891 ± 0.067	0.871 ± 0.05	0.857 ± 0.046	0.856 ± 0.047	0.856 ± 0.054	0.851 ± 0.05	0.858 ± 0.049
	FedProx μ = 2 MLP	0.868 ± 0.06	0.866 ± 0.072	0.876 ± 0.072	0.881 ± 0.066	0.881 ± 0.066	0.882 ± 0.059	0.884 ± 0.053	0.874 ± 0.064	0.877 ± 0.056

Data reported are mean and standard deviation across K = 6-fold cross-validation. Best performing algorithms for each metric are indicated by an asterisk.

Table 4. AUC-PR score of models trained using federated learning as the quantity of client sites increased, tested on the PDBP dataset

		Number of clients								
		2	4	6	8	10	12	14	16	18
Algorithm name	FedAvg LR	0.826 ± 0.011	0.811 ± 0.011	0.805 ± 0.01	0.8 ± 0.016	0.797 ± 0.017	0.799 ± 0.016	0.804 ± 0.018	0.799 ± 0.022	0.794 ± 0.021
	FedAvg MLP	0.78 ± 0.012	0.801 ± 0.014	0.79 ± 0.013	0.791 ± 0.015	0.803 ± 0.008	0.782 ± 0.017	0.793 ± 0.006	0.778 ± 0.005	0.781 ± 0.009
	FedAvg SGD	0.847 ± 0.008	0.823 ± 0.009	0.821 ± 0.009	0.822 ± 0.009	0.806 ± 0.016	0.81 ± 0.006	0.804 ± 0.013	0.805 ± 0.009*	0.798 ± 0.014
	FedAvg XGBRF	0.876 ± 0.009*	0.858 ± 0.016*	0.856 ± 0.019*	0.834 ± 0.02*	0.824 ± 0.018*	0.821 ± 0.018*	0.807 ± 0.034*	0.775 ± 0.051	0.752 ± 0.054
	FedProx μ = 0 LR	0.823 ± 0.015	0.825 ± 0.005	0.807 ± 0.012	0.801 ± 0.016	0.797 ± 0.018	0.803 ± 0.018	0.793 ± 0.021	0.802 ± 0.019	0.8 ± 0.022*
	FedProx μ = 0 MLP	0.791 ± 0.006	0.803 ± 0.012	0.795 ± 0.014	0.789 ± 0.011	0.796 ± 0.011	0.794 ± 0.009	0.787 ± 0.007	0.79 ± 0.008	0.778 ± 0.011
	FedProx μ = 2 LR	0.835 ± 0.007	0.812 ± 0.007	0.809 ± 0.006	0.8 ± 0.013	0.796 ± 0.018	0.796 ± 0.018	0.793 ± 0.02	0.802 ± 0.019	0.789 ± 0.023
	FedProx μ = 2 MLP	0.785 ± 0.015	0.8 ± 0.012	0.788 ± 0.01	0.792 ± 0.01	0.797 ± 0.007	0.791 ± 0.01	0.793 ± 0.008	0.784 ± 0.009	0.791 ± 0.011

Data reported are mean and standard deviation across K = 6-fold cross-validation. Best performing algorithms for each metric are indicated by an asterisk.
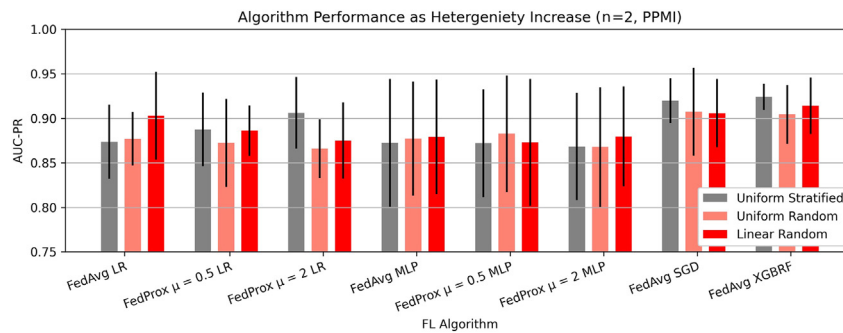
Figure 5. Data heterogeneity at client sites does not deeply influence model performance
The AUC-PR for a federation of two clients for several split methods. Uniform stratified sampling represents the most homogeneous data-distribution method, while uniform random and linear random represent increasingly heterogeneous client distributions. Presented data are mean score and standard deviation resulting from cross-validation.

algorithms using MLP as a local learner. The progressive increase in runtime may be attributed to the relative difference in complexity between the FedAvg and FedProx optimization mechanism. The objective of FedProx weight aggregation function includes a regularization term, μ, designed to handle heterogeneity among clients.[19] The FedAvg optimization objective does not include this mechanism, making it conceptually simpler. In the context of this study, the performance differences incurred by choice in aggregation method are minor relative to parameters such as choice in local learner, number of federated aggregation rounds, and dataset size.

When comparing the training time of central and federated models, we find that the central model training time is at least an order of magnitude lower than the federated training time. This result is not surprising, given that federated models implement global weight aggregation and updating steps in model training. Given that our study performs federated optimization in simulation, production deployments of FL methods can be expected to have slower overall runtimes due to network latency and operating system throughput capabilities.

The algorithms used in evaluating collaboratively trained models using FL against centralized applications of their local learner methods are detailed in Table S2. In our study, we omitted using closed-source FL methods available through platform interfaces, since these methods allow data governance capabilities to external parties or vendor security evaluations, which in some cases instantiate barriers to productive research. While numerous publications explore methodological improvements that push forward state-of-the-art FL model performance in an experimental setting, we encountered challenges in applying such methods in our case, as many of these academic studies do not result in broadly applicable packages. In our research, we found a set of open-source projects that implement FL methods and provide out-of-the-box solutions or well-designed examples that could be interpolated to the multi-omics classification task to be limited. Ultimately, the FL interfaces made available by NVFlare[32] and Flower[33] were selected to conduct experiments, with local learners implemented using Sklearn[22] and DMLC[21] packages. Several open-source projects, such as Owkin,[34] Tensorflow Federated,[35] and OpenFL,[36] provide full interfaces for implementing deep-learning models in TensorFlow[35] and PyTorch,[37] but such deep methods are less suitable for tabular tasks on datasets with only a handful of samples, as is the case for the multi-omics datasets used in this study. Additionally, we found that while several packages provided abstract interfaces for implementing any arbitrary set of local learners and aggregation strategies, without detailed

examples with a straightforward path to adaptation to a particular research task, the practical application of such methods becomes challenging and less approachable for groups which may be resource constrained.

The extent to which federation site configurations could be studied was largely limited by the number of case patients within the dataset. Concretely, the implications of heterogeneity in site data could only be observed to the extent that each silo would maintain enough samples from case and control cohorts to allow the local learner to successfully train. Datasets at silos needed to have at least one sample from both the case and control groups. Similarly, although the PPMI dataset was collected across several geographically distributed institutions, point-of-origin information is not available for each sample, preventing the evaluation of performance on naturally occurring silos. In our study, all experiments assume that the collective dataset available among all client sites has a constant size. An additional limitation of our work is in observing the effect of adding federation members, which contribute novel samples to the federation.

While FL methods enable data owners to maintain governance of their local datasets, on its own FL does not provide end-to-end privacy guarantees. Our study examines the utility of FL methods in the multi-omics case study to understand the availability and characteristics of FL and does not include a concrete evaluation of privacy or security methods. Thus, we assume that the FL aggregation server is neither dishonest, curious, nor malicious in any way and fulfills its functions as an intermediary between client sites benevolently. Privacy-preserving methods orthogonal to FL such as differential privacy (DP) enable the application of FL with formal guarantees of sample privacy.[38] Such approaches were not included in the scope of this evaluation but represent a factor which should be considered when applying FL methods in settings where verifiable sample-privacy guarantees are critical. In our experimentation, we do not focus on the implications of the federation that has heterogeneous compute capabilities, since applying ML model fitting on datasets with few samples can be done without much difficulty.

The datasets utilized in our analysis, including PPMI and PDBP, are sourced from the Accelerating Medicines Partnership Parkinson's Disease (AMP-PD) initiative. This initiative plays a pivotal role in unifying transcriptomic and genomic samples, ensuring consistency and accuracy through central harmonization and joint-calling processes. Furthermore, the construction of ML features for our analysis is also centralized, leveraging these cohesive datasets. Recognizing the potential for broader application, our future focus includes exploring federated analysis tasks.[39–41]
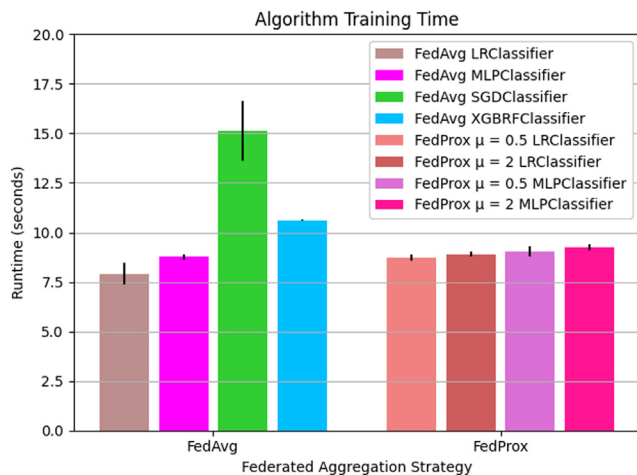
Algorithm Training Time

Figure 6. The mean runtime to train FL models using FedAvg and FedProx strategies

The mean total runtime in seconds to train FL models. FL models are trained on the PPMI training folds for five communication rounds. Algorithms are grouped by aggregation strategy. Results presented as mean and standard deviation over $K = 6$ folds.

This involves enhancing cross-silo harmonization, joint-calling, and feature construction across diverse datasets. To facilitate this, the development of specialized FL libraries, specifically tailored for genomics and transcriptomics, is crucial. Such advancements will not only democratize access to FL methods for the wider biomedical community but also significantly broaden the scope for applying ML techniques in various biomedical contexts.

Overall, we believe that this work sheds light on the feasibility and noteworthy characteristics of applying FL for omics analysis. Through our experiments, we find that collaboratively trained FL models can achieve high classification accuracy in multi-omics Parkinson's disease diagnosis and can remain relatively performant despite heterogeneity among client sites. We also find in our evaluation that although FL is a relatively novel research space in bioinformatics, there is sufficient access to open-source methods which biomedical researchers may leverage to enable productive collaborations.

EXPERIMENTAL PROCEDURES

Resource availability

Lead contact

Further information and requests for resources and reagents should be directed to and will be fulfilled by the lead contact, Faraz Faghri (faraz@datatecnica.com).

Materials availability

This study did not generate new unique materials.

Data and code availability

Data: the data used in this study was access-controlled from the PPMI (http://www.ppmi-info.org/) and the PDBP (https://pdbp.ninds.nih.gov/).

Code: to facilitate replication and expansion of our work, we have made the notebook publicly available in an open repository.[42] It includes all code, figures, models, and supplements for this study. The code is part of the supplemental information; it includes the rendered Jupyter notebook with full step-by-step data preprocessing, statistical, and ML analysis.

Any additional information required to reanalyze the data reported in this paper is available from the lead contact upon request. All authors and the public

Table 5. Total runtime in seconds to train central and federated models, averaged over K folds

	Algorithm name	Runtime (s)
Central	Logistic regression	$1.857e{-}02 \pm 0.008$
	SGD classifier	$6.771e{-}03 \pm 0.001$*
	MLP classifier	$1.609e{-}01 \pm 0.009$
	XGBRF classifier	$1.633e{-}01 \pm 0.003$
FedAvg	FedAvg SGD classifier	$1.513e{+}01 \pm 1.497$
	FedAvg XGBRF classifier	$1.061e{+}01 \pm 0.014$
	FedAvg LR classifier	$7.909e{+}00 \pm 0.550$*
	FedAvg MLP classifier	$8.755e{+}00 \pm 0.141$
FedProx	FedProx $\mu = 0.5$ LR classifier	$8.747e{+}00 \pm 0.158$*
	FedProx $\mu = 0.5$ MLP classifier	$9.039e{+}00 \pm 0.266$
	FedProx $\mu = 2$ LR classifier	$8.905e{+}00 \pm 0.130$
	FedProx $\mu = 2$ MLP classifier	$9.260e{+}00 \pm 0.163$

Algorithms are grouped by aggregation strategy (central, FedAvg, FedProx). The lowest training time for each group is bolded. Best performing algorithms for each metric are indicated by an asterisk.

can access all data and statistical programming code used in this project for the analyses and results generation.

Datasets

The dataset used in this study as the basis for training and as the internal test set is the PPMI dataset, which represents a longitudinal observational study where patients contribute clinical, demographic, imaging data, and biological samples for whole-genome sequencing and whole-blood RNA sequencing. Samples are collected at 33 clinical sites globally and across a time span of anywhere from 5 to 13 years. This preprocessed dataset consists of 171 samples of case patients diagnosed with Parkinson's disease and 427 healthy control patients. The PPMI cohort contains newly diagnosed and drug-naive patient samples. The cohort contains 209 (36%) female samples and 388 (67%) male samples (Table S4).

The dataset used in this study for external, out-of-distribution validation is the PDBP, a longitudinal, observational study where patients contribute clinical, demographic, and imaging data and biological samples for whole-genome and whole-blood RNA sequencing. The preprocessed dataset consists of 712 healthy control patients and 404 case patients diagnosed with Parkinson's disease. Each sample comprises 713 features, including genetic, transcriptomic, and clinico-demographic information collected at the baseline. The PDBP cohort consists of 480 (43%) female samples and 636 (57%) male samples (Table S5).

Both PPMI and PDBP data used in this study were acquired through the AMP-PD initiative,[43] an effort to provide harmonized datasets that include common clinical and genomic data. Through this initiative, the PPMI and PDBP datasets are centrally joint-called and harmonized to allow standardization across cohorts.

Transcriptomic data from whole-blood RNA sequencing was generated by the Translational Genomics Research Institute team using standard protocols for the Illumina NovaSeq technology and processed through variance-stabilization and limma pipelines[44] for experimental covariates. Gene expression counts for protein-coding genes were extracted, then differential expression p values were calculated between cases and controls using LR adjusted for additional covariates of sex, plate, age, ten principal components, and percentage usable bases. A comprehensive description of the RNA-sequencing method is presented in Hutchins et al.[45] for PPMI and Gwinn et al.[46] for PDBP.

For genetic data, sequencing data were generated using Illumina's standard short-read technology, and the functional equivalence pipeline during alignment was the Broad Institute's implementation.[47] Applied quality control measures included criteria such as gender concordance and call rate, with a focus on SNPs meeting the GATK gold-standards pipeline and additional filters such as non-palindromic alleles and missingness by case-control status thresholds. Polygenic risk scores (PRSs) were constructed using effect sizes from a large European genome-wide meta-analysis, supplementing the genetic data from

whole-genome sequences. The process from sample preparation to variant calling is comprehensively described in Iwaki et al.[43]

Quality control for genetic samples based on genetic data output by the pipeline included the following inclusion criteria: concordance between genetic and clinically ascertained genders, call rate >95% at both the sample and variant levels, heterozygosity rate <15%, free mix estimated contamination rate <3%, transition/transversion ratio >2, unrelated to any other sample at a level of the first cousin or closer (identity by descent <12.5%), and genetically ascertained European ancestry. For inclusion of whole-genome DNA-sequencing data, the variants must have passed basic quality control as part of the initial sequencing effort (PASS flag from the joint genotyping pipeline) as well as meeting the following criteria: non-palindromic alleles, missingness by case-control status p > 1e−4, missingness by haplotype p > 1e−4, Hardy-Weinberg p value >1e−4, minor allele frequency in cases >5% (in the latest Parkinson's disease meta-genome-wide association study (meta-GWAS) by Nalls et al.[48]). As an a priori genetic feature to be included in our modeling efforts, we also used the basic polygenic risk score from the latest Parkinson's disease meta-GWAS (genome-wide significant loci only) that did not include our testing or training samples as weights.[48]

Compared to the PPMI dataset, PDBP includes an additional 40 genetic features, which are excluded from this study, allowing PPMI and PDBP to have the same feature set. Additionally, the PPMI samples are collected before any medical intervention, whereas the PDBP samples are, in some cases, collected after patient treatment has commenced. Since the PDBP dataset may include artifacts that result from disease treatment, the PDBP dataset is used exclusively for evaluation to avoid the possibility of label leakage. A shortened version of the final feature set is provided in Table S1. A comprehensive feature list is available in the external code repository.[42]

Each sample consists of 673 features, including genetic, transcriptomic, and clinico-demographic information collected at the baseline. Of the 673 features, 72 originate from genome-sequencing data and PRS, 596 are transcriptomic, and 5 are clinico-demographic. The clinico-demographic features include age, family history, inferred Ashkenazi Jewish status, sex, and University of Pennsylvania Smell Identification (UPSIT) score.

Data preprocessing

The construction of features from genomic, transcriptomic, and clinico-demographic data is handled for each cohort independently, and in a centralized manner, for the entirety of the cohort. As part of the initial data preprocessing, principal components summarizing genetic variation in DNA- and RNA-sequencing data modalities were generated separately. For the DNA sequencing, ten principal components were calculated based on a random set of 10,000 variants sampled after linkage disequilibrium (LD) pruning that kept only variants with $r^2 < 0.1$ with any other variants in ±1 MB. As a note, these variants were not p valuefiltered based on recent GWAS, but they do exclude regions containing large tracts of LD.[49] Our genetic data pruning removed SNPs in long tracts of high LD such as in the HLA region (we excluded any SNPs within $r^2 > 0.1$ within a sliding window of 1 MB) while retaining known genetic risk SNPs within the region. For RNA-sequencing data, all protein-coding genes' read counts per sample were used to generate a second set of ten principal components. All potential features representing genetic variants (in the form of minor allele dosages) from sequencing were then adjusted for the DNA-sequence-derived principal components using linear regression, extracting the residual variation. This adjustment removes the effects of quantifiable European population substructure from the genetic features prior to training; this is similar in theory to adjusting analyses for the same principal components in the common variant regression paradigm employed by GWAS models. The same was done for RNA-sequencing data using RNA-sequencing-derived principal components. This way, we statistically account for latent population substructure and experimental covariates at the feature level to increase generalizability across heterogeneous datasets. In its simplest terms, all transcriptomic data were corrected for possible confounders, and the same is done for genotype dosages. After adjustment, all continuous features were then Z-transformed to have a mean of 0 and a standard deviation of 1 to keep all features on the same numeric scale when possible. Once feature adjustment and normalization were complete, internal feature selection was carried out in the PPMI training dataset using decision trees (extraTrees classifier) to identify features contributing information content to the model while reducing the potential for overfitting prior to model generation.[22,50] Overfitting here is defined

as the overperformance of a model in the training phase with minimal generalizability in the validation dataset due to the inclusion of potentially correlated or unimportant features. The implementation of decision trees for feature selection helps remove redundant and low-impact features, helping us to generate the most parsimonious feature set for modeling. Feature selection was run on combined data modalities to remove potentially redundant feature contributions that could artificially inflate model accuracy. Export estimates for features most likely to contribute to the final model in order of importance were generated by the extraTrees classifier for each of the combined models and are available on the online repository. By removing redundant features, the potential for overfitting is limited while also making the models more conservative. Additionally, if a variant provided redundant model information, such as being in strong linkage with a PRS variant, it would be removed from the potential feature list.

Feature selection was performed using the extremely randomized trees classifier algorithm, extraTrees,[50] on combined data modalities to remove redundant feature contributions that could overfit the model to optimize the information content from the features and limit artificial inflation in predictive accuracy that might be introduced by including such a large number of features before filtering. In many cases, including more data might not be better for performance. With this in mind, we attempted to build the most parsimonious model possible using systematic feature selection criteria.[51] Among the top 5% of features ranked in the Shapley analysis, the mean correlation between features was $r^2 < 5\%$, with a maximum of 36%. By removing redundant features using correlation-based pruning and an extraTrees classifier as a data-munging step, the potential for overfitting is limited while also making the models more conservative.

Clinical and demographic data ascertained as part of this project included age at diagnosis for cases and age at baseline visit for controls. Family history (self-reporting if a first or second-degree relative has a diagnosis of Parkinson's disease) was also a known clinico-demographic feature of interest. Ashkenazi Jewish status was inferred using principal component analysis comparing those samples to a genetic reference series, referencing the genotyping array data from GSE23636 at the Gene Expression Omnibus as previously described elsewhere.[43,52] Sex was clinically ascertained but also confirmed using X chromosome heterozygosity rates. The UPSIT was used in modeling.[53] A comprehensive description of data and preprocessing is described in Makarious et al.[6]

Quantification and statistical analysis

We conducted K-fold cross-validation on the PPMI dataset, where $K = 6$, allowing each fold to contain approximately 100 samples. For each cross-validation fold, $1/K$ of the PPMI samples are withheld as a holdout test set. The remaining training split of $K − 1/K$ samples are further split using uniform stratified random sampling at an 80:20 ratio into training and validation subsets. The evaluation set was used for cross-validated hyperparameter tuning in the central and federated models. The PPMI dataset was selected as the training and internal test set due to the fact that patient samples recorded in the PPMI protocol are newly diagnosed and drug naive. Additionally, by training on the PPMI dataset, the model is developed on patients earlier on in their disease course. This intentional choice was made in the hope that the model would identify other individuals early on in their disease course and prioritize them for follow-up. The PDBP cohort samples are collected within 5 years after diagnosis, and these patients may be actively taking medications. While the PDBP cohort is larger, because samples are collected several years after diagnosis and because patients may be actively taking medication, there is a possibility of label leakage, ultimately motivating the usage of the PPMI dataset for training. Due to the similar nature of the PPMI and PDBP datasets, after processing, the PDBP dataset can be used as an external test set, approximating out-of-distribution model performance.

To conduct federated model training, the fully preprocessed PPMI dataset is split into disjoint client subsets, using one of the split strategies, and assigned to a local learner. To train a global model using the data among all federation participants, an iterative optimization process is run for a predefined set of rounds (Figure 2). During this process, federation members fit local learner models to their locally available datasets. The parameters resulting from local model fitting are then sent to the central aggregation server. Once all model parameters are received, the aggregation server applies a FL strategy to the set of model weights, resulting in aggregated model weights, referred to as the global model. The global model is then sent back to the client sites and used as the starting point for local learner optimization in subsequent iterations. The best-performing global model on the evaluation set is used for final testing.

We simulate two types of heterogeneity in our experiments by distributing samples from the training dataset using different split methods. Split-method uniform stratified sampling implements label and site-size homogeneity. Split-method uniform random sampling implements label heterogeneity but site-size homogeneity. Split-method linear random sampling implements label- and site-size heterogeneity (Figure 3).

Local client datasets were formed by applying such sampling techniques to the centralized training dataset. Uniform stratified sampling was used to form the K folds and during experiments that study homogeneous federations. Uniform stratified sampling entails sampling the source dataset such that there is a nearly even distribution of samples among each of the n clients, and the ratio of cases to controls across each client subset is equivalent (where surplus samples are assigned to one of the client sites at random). This method was implemented by partitioning the source dataset by phenotype and then, without replacement, assigning 1/N samples of each phenotype partition to each client using uniform random sampling, with the last client receiving any extra samples. In practice, this additional data was fewer than ten of the samples. Uniform random sampling entails assigning 1/N using uniform random sampling. Linear random sampling entails assigning c_i samples to a client site, where the following is true:

$$\sum_{i=1}^{N} i * c_i = C.$$

In the above formula, C is the number of samples to distribute, in practice the size of the PPMI training set, and i is the index of the client site. As with previous methods, the final client receives any surplus samples left over. The effect of this linear random sampling strategy is that each of the n clients contains an increasing number of samples relative to the previous clients, and each client site contains a random distribution of cases versus controls.

To measure algorithm runtime, for central algorithms we measured the quantity of seconds from model initialization to model training completion. For federated algorithms, we measured the quantity of seconds from model initialization to the end of the FL training simulation. For FL models, model optimization was conducted for a federation of n = 2 federation clients for five aggregation rounds.

In our simulation configurations, federation rounds operate synchronously and without failure. Hyperparameters that were used to compute the final results are reported in the supplemental information, including the random seed used for the presented results.

The federated ML methods implemented in the study utilize the federated aggregation methods FedAvg,[18] FedProx,[19] and the local learner classification methods LR,[17] Multi-Layer Perceptron,[20] Stochastic Gradient Descent,[23] and XGBoost[21] available through Sklearn[22] and DMLC.[21,22] The aggregation methods are implemented using NVFlare[32] and Flower,[33] while local learner methods are implemented using Sklearn and DMLC APIs. Configuration details are available in the supplemental information. Simulation frameworks used to implement model experiments are made available through the NVFlare and Flower packages. A single client site exhibits a minor computational cost of a single GB CPU and a single logical processor, which must be available throughout the life of the simulation. The simulations for both NVFlare and Flower required 18 GB of RAM and 18 logical cores. A simulation to train a single FL model takes less than 1 min to complete. Running the full suite of simulations to reproduce the paper figures takes 6–8 h. All experiments were conducted on Redhat Enterprise Linux Distribution.

SUPPLEMENTAL INFORMATION

Supplemental information can be found online at https://doi.org/10.1016/j.patter.2024.100945.

AUTHOR CONTRIBUTIONS

B.P.D., M.B.M., A.D., D.V., A.B.S., M.A.N., J.S., and F.F. contributed to the concept and design of the study. B.P.D., M.B.M., A.D., D.V., M.A.N., and F.F. were involved in the acquisition of data, data generation, and data cleaning. B.P.D., A.D., M.A.N., and F.F. carried out the analysis and interpretation of data. B.P.D., M.B.M., A.D., D.V., P.S.L., A.B.S., M.A.N., J.S., and F.F. contributed to the drafting of the article and revising it critically.

REFERENCES

1. Dadu, A., Satone, V., Kaur, R., Hashemi, S.H., Leonard, H., Iwaki, H., Makarious, M.B., Billingsley, K.J., Bandres-Ciga, S., Sargent, L.J., et al. (2022). Identification and prediction of Parkinson's disease subtypes and progression using machine learning in two cohorts. NPJ Parkinsons Dis. 8, 172. https://doi.org/10.1038/s41531-022-00439-z.

2. Prashanth, R., Dutta Roy, S., Mandal, P.K., and Ghosh, S. (2016). High-Accuracy Detection of Early Parkinson's Disease through Multimodal Features and Machine Learning. Int. J. Med. Inf. 90, 13–21. https://doi.org/10.1016/j.ijmedinf.2016.03.001.

3. Pantaleo, E., Monaco, A., Amoroso, N., Lombardi, A., Bellantuono, L., Urso, D., Lo Giudice, C., Picardi, E., Tafuri, B., Nigro, S., et al. (2022). A Machine Learning Approach to Parkinson's Disease Blood Transcriptomics. Genes 13. https://doi.org/10.3390/genes13050727.

4. Lee, D.A., Lee, H.-J., Kim, H.C., and Park, K.M. (2022). Application of machine learning analysis based on diffusion tensor imaging to identify REM sleep behavior disorder. Sleep Breath. 26, 633–640. https://doi.org/10.1007/s11325-021-02434-9.

5. Green, E.D., Gunter, C., Biesecker, L.G., Di Francesco, V., Easter, C.L., Feingold, E.A., Felsenfeld, A.L., Kaufman, D.J., Ostrander, E.A., Pavan, W.J., et al. (2020). Strategic vision for improving human health at The

Forefront of Genomics. Nature *586*, 683–692. https://doi.org/10.1038/s41586-020-2817-4.

6. Makarious, M.B., Leonard, H.L., Vitale, D., Iwaki, H., Sargent, L., Dadu, A., Violich, I., Hutchins, E., Saffo, D., Bandres-Ciga, S., et al. (2022). Multi-modality machine learning predicting Parkinson's disease. NPJ Parkinsons Dis. *8*, 35. https://doi.org/10.1038/s41531-022-00288-w.

7. Kim, J.J., Vitale, D., Véliz Otani, D., Lian, M., Heilbron, K., the 23andMe Research Team, Iwaki, H., Lake, J., Solsberg, C.W., Leonard, H., et al. (2022). Multi-ancestry genome-wide meta-analysis in Parkinson's disease (Genetic and Genomic Medicine). Preprint at medRxiv. https://doi.org/10.1038/s41588-023-01584-8.

8. Antunes, R.S., André da Costa, C., Küderle, A., Yari, I.A., and Eskofier, B. (2022). Federated Learning for Healthcare: Systematic Review and Architecture Proposal. ACM Trans. Intell. Syst. Technol. *13*, 1–23. https://doi.org/10.1145/3501813.

9. McMahan, H.B., Moore, E., Ramage, D., and Hampson, S. (2017). Communication-Efficient Learning of Deep Networks from Decentralized Data. In Proceedings of the 20th International Conference on Artificial Intelligence and Statistics Proceedings of Machine Learning Research, S.A.A. Jerry, ed. (PMLR), pp. 1273–1282.

10. Dash, B., Sharma, P., and Ali, A. (2022). Federated Learning for Privacy-Preserving: A Review of PII Data Analysis in Fintech. International Journal of Software Engineering & Applications (IJSEA) *13*, 1–13.

11. Sheller, M.J., Edwards, B., Reina, G.A., Martin, J., Pati, S., Kotrotsou, A., Milchenko, M., Xu, W., Marcus, D., Colen, R.R., and Bakas, S. (2020). Federated learning in medicine: facilitating multi-institutional collaborations without sharing patient data. Sci. Rep. *10*, 12598. https://doi.org/10.1038/s41598-020-69250-1.

12. Xu, J., Glicksberg, B.S., Su, C., Walker, P., Bian, J., and Wang, F. (2021). Federated Learning for Healthcare Informatics. J. Healthc. Inform. Res. *5*, 1–19. https://doi.org/10.1007/s41666-020-00082-4.

13. Oldenhof, M., Ács, G., Pejó, B., Schuffenhauer, A., Holway, N., Sturm, N., Dieckmann, A., Fortmeier, O., Boniface, E., Mayer, C., et al. (2023). Industry-Scale Orchestrated Federated Learning for Drug Discovery. AAAI *37*, 15576–15584. https://doi.org/10.1609/aaai.v37i13.26847.

14. Dayan, I., Roth, H.R., Zhong, A., Harouni, A., Gentili, A., Abidin, A.Z., Liu, A., Costa, A.B., Wood, B.J., Tsai, C.-S., et al. (10/2021). Federated learning for predicting clinical outcomes in patients with COVID-19. Nat. Med. *27*, 1735–1743. https://doi.org/10.1038/s41591-021-01506-3.

15. Lee, G.H., and Shin, S.-Y. (2020). Federated Learning on Clinical Benchmark Data: Performance Assessment. J. Med. Internet Res. *22*, e20891. https://doi.org/10.2196/20891.

16. Beguier, C., Terrail, J.O. du, Meah, I., Andreux, M., and Tramel, E.W. (2021). Differentially Private Federated Learning for Cancer Prediction. Preprint at arXiv. https://doi.org/10.48550/arXiv.2101.02997.

17. Cox, D.R. (1958). The regression analysis of binary sequences. J. Roy. Stat. Soc. *20*, 215–232. https://doi.org/10.1111/j.2517-6161.1958.tb00292.x.

18. McMahan, H.B., Moore, E., Ramage, D., Hampson, S., and Arcas, B.A.y. (2023). Communication-Efficient Learning of Deep Networks from Decentralized Data. Preprint at arXiv. https://doi.org/10.48550/arXiv.1602.05629.

19. Li, T., Sahu, A.K., Zaheer, M., Sanjabi, M., Talwalkar, A., and Smith, V. (2018). Federated Optimization in Heterogeneous Networks. Preprint at arXiv. https://doi.org/10.48550/arXiv.1812.06127.

20. Haykin, S. (1998). Neural Networks: A Comprehensive Foundation, 2nd ed. (Prentice Hall PTR).

21. Chen, T., and Guestrin, C. (2016). XGBoost: A Scalable Tree Boosting System. In Proceedings of the 22nd ACM SIGKDD International Conference on Knowledge Discovery and Data Mining, pp. 785–794. https://doi.org/10.1145/2939672.2939785.

22. Pedregosa, F., Varoquaux, G., Gramfort, A., Michel, V., Thirion, B., Grisel, O., Blondel, M., Müller, A., Nothman, J., Louppe, G., et al. (2012). Scikit-learn: Machine Learning in Python. Preprint at arXiv. https://doi.org/10.48550/arXiv.1201.0490.

23. Cortes, C., and Vapnik, V. (1995). Support-vector networks. Mach. Learn. *20*, 273–297. https://doi.org/10.1007/BF00994018.

24. Ng, D., Lan, X., Yao, M.M.-S., Chan, W.P., and Feng, M. (2021). Federated learning: a collaborative effort to achieve better medical imaging models for individual sites that have small labelled datasets. Quant. Imag. Med. Surg. *11*, 852–857. https://doi.org/10.21037/qims-20-595.

25. Kairouz, P., McMahan, H.B., Avent, B., Bellet, A., Bennis, M., Bhagoji, A.N., Bonawitz, K., Charles, Z., Cormode, G., Cummings, R., et al. (2021). Advances and Open Problems in Federated Learning. Preprint at arXiv. https://doi.org/10.48550/arXiv.1912.04977.

26. Menze, B.H., Jakab, A., Bauer, S., Kalpathy-Cramer, J., Farahani, K., Kirby, J., Burren, Y., Porz, N., Slotboom, J., Wiest, R., et al. (2015). The Multimodal Brain Tumor Image Segmentation Benchmark (BRATS). IEEE Trans. Med. Imag. *34*, 1993–2024. https://doi.org/10.1109/TMI.2014.2377694.

27. Pati, S., Baid, U., Edwards, B., Sheller, M., Wang, S.-H., Reina, G.A., Foley, P., Gruzdev, A., Karkada, D., Davatzikos, C., et al. (2022). Federated learning enables big data for rare cancer boundary detection. Nat. Commun. *13*, 7346.

28. Ge, S., Wu, F., Wu, C., Qi, T., Huang, Y., and Xie, X. (2020). FedNER: Privacy-preserving Medical Named Entity Recognition with Federated Learning. Preprint at arXiv. https://doi.org/10.48550/arXiv.2003.09288.

29. Salmeron, J.L., Arévalo, I., and Ruiz-Celma, A. (2023). Benchmarking federated strategies in Peer-to-Peer Federated learning for biomedical data. Heliyon *9*, e16925. https://doi.org/10.1016/j.heliyon.2023.e16925.

30. Ledell, E., and Poirier, S. (2020). H2O AutoML: Scalable Automatic Machine Learning. https://www.automl.org/wp-content/uploads/2020/07/AutoML_2020_paper_61.pdf.

31. Feurer, M., Klein, A., Eggensperger, K., Springenberg, J., Blum, M., and Hutter, F. (2015). Efficient and robust automated machine learning. In Advances in Neural Information Processing Systems 28 (NIPS, C. Cortes, N. Lawrence, D. Lee, M. Sugiyama, and R. Garnett, eds. (Curran Associates, Inc.).

32. Roth, H.R., Cheng, Y., Wen, Y., Yang, I., Xu, Z., Hsieh, Y.-T., Kersten, K., Harouni, A., Zhao, C., Lu, K., et al. (2022). NVIDIA FLARE: Federated Learning from Simulation to Real-World. Preprint at arXiv. https://doi.org/10.48550/arXiv.2210.13291.

33. Beutel, D.J., Topal, T., Mathur, A., Qiu, X., Fernandez-Marques, J., Gao, Y., Sani, L., Li, K.H., Parcollet, T., de Gusmão, P.P.B., et al. (2020). Flower: A Friendly Federated Learning Research Framework. Preprint at arXiv. https://doi.org/10.48550/arXiv.2007.14390.

34. Galtier, M.N., and Marini, C. (2019). Substra: a framework for privacy-preserving, traceable and collaborative Machine Learning. Preprint at arXiv. https://doi.org/10.48550/arXiv.1910.11567.

35. Dean, J., and Monga 'TensorFlow, R. (2015). Large-Scale Machine Learning on Heterogeneous Distributed Systems'. Preprint at arXiv. https://doi.org/10.48550/arXiv.1603.04467.

36. Foley, P., Sheller, M.J., Edwards, B., Pati, S., Riviera, W., Sharma, M., Narayana Moorthy, P., Wang, S.-H., Martin, J., Mirhaji, P., et al. (2022). OpenFL: the open federated learning library. Phys. Med. Biol. *67*, 214001. https://doi.org/10.1088/1361-6560/ac97d9.

37. Paszke, A., Gross, S., Massa, F., Lerer, A., Bradbury, J., Chanan, G., Killeen, T., Lin, Z., Gimelshein, N., Antiga, L., et al. (2019). PyTorch: An Imperative Style, High-Performance Deep Learning Library. In 33rd Conference on Neural Information Processing Systems, pp. 8026–8037.

38. Abadi, M., Chu, A., Goodfellow, I., McMahan, H.B., Mironov, I., Talwar, K., and Zhang, L. (2016). Deep Learning with Differential Privacy. In Proceedings of the 2016 ACM SIGSAC Conference on Computer and Communications Security CCS '16 (Association for Computing Machinery), pp. 308–318. https://doi.org/10.1145/2976749.2978318.

39. Elkordy, A.R., Ezzeldin, Y.H., Han, S., Sharma, S., He, C., Mehrotra, S., and Avestimehr, S. (2023). Federated Analytics: A Survey. APSIPA Trans. Signal Inf. Process. *12*. https://doi.org/10.1561/116.00000063.

40. Froelicher, D., Troncoso-Pastoriza, J.R., Raisaro, J.L., Cuendet, M.A., Sousa, J.S., Cho, H., Berger, B., Fellay, J., and Hubaux, J.-P. (2021).

Truly privacy-preserving federated analytics for precision medicine with multiparty homomorphic encryption. Nat. Commun. *12*, 5910. https://doi.org/10.1038/s41467-021-25972-y.

41. Wang, J., Charles, Z., Xu, Z., Joshi, G., Brendan McMahan, H., Aguera y Arcas, B., Al-Shedivat, M., Andrew, G., Avestimehr, S., Daly, K., et al. (2021). A Field Guide to Federated Optimization. Preprint at arXiv. https://doi.org/10.48550/arXiv.2107.06917.

42. Danek, B., Lee, P.S., Makarious, M., Dadu, A., Vitale, D., Paul Suhwan, L., Nalls, M., Sun, J., and Faghri, F. (2023). BPDanek/multi-omics-pdd-FL-study. Public Release (Zenodo). https://doi.org/10.5281/ZENODO.10430973.

43. Iwaki, H., Leonard, H.L., Makarious, M.B., Bookman, M., Landin, B., Vismer, D., Casey, B., Gibbs, J.R., Hernandez, D.G., Blauwendraat, C., et al. (2021). Accelerating Medicines Partnership: Parkinson's Disease. Mov. Disord. *36*, 1795–1804. https://doi.org/10.1002/mds.28549.

44. Ritchie, M.E., Phipson, B., Wu, D., Hu, Y., Law, C.W., Shi, W., and Smyth, G.K. (2015). limma powers differential expression analyses for RNA-sequencing and microarray studies. Nucleic Acids Res. *43*, e47. https://doi.org/10.1093/nar/gkv007.

45. Hutchins, E., Craig, D., Violich, I., Alsop, E., Casey, B., Hutten, S., Reimer, A., Whitsett, T.G., Crawford, K.L., Toga, A.W., et al. (2021). Quality control metrics for whole blood transcriptome analysis in the Parkinson's Progression Markers Initiative (PPMI). Preprint at arXiv. https://doi.org/10.1101/2021.01.05.21249278.

46. Gwinn, K., David, K.K., Swanson-Fischer, C., Albin, R., Hillaire-Clarke, C.S., Sieber, B.-A., Lungu, C., Bowman, F.D., Alcalay, R.N., Babcock, D., et al. (2017). Parkinson's disease biomarkers: perspective from the NINDS Parkinson's Disease Biomarkers Program. Biomarkers Med. *11*, 451–473. https://doi.org/10.2217/bmm-2016-0370.

47. Regier, A.A., Farjoun, Y., Larson, D.E., Krasheninina, O., Kang, H.M., Howrigan, D.P., Chen, B.-J., Kher, M., Banks, E., Ames, D.C., et al. (2018). Functional equivalence of genome sequencing analysis pipelines enables harmonized variant calling across human genetics projects. Nat. Commun. *9*, 4038. https://doi.org/10.1038/s41467-018-06159-4.

48. Nalls, M.A., Blauwendraat, C., Vallerga, C.L., Heilbron, K., Bandres-Ciga, S., Chang, D., Tan, M., Kia, D.A., Noyce, A.J., Xue, A., et al. (2019). Identification of novel risk loci, causal insights, and heritable risk for Parkinson's disease: a meta-analysis of genome-wide association studies. Lancet Neurol. *18*, 1091–1102. https://doi.org/10.1016/S1474-4422(19)30320-5.

49. Abraham, G., Qiu, Y., and Inouye, M. (2017). FlashPCA2: principal component analysis of Biobank-scale genotype datasets. Bioinformatics *33*, 2776–2778. https://doi.org/10.1093/bioinformatics/btx299.

50. Geurts, P., Ernst, D., and Wehenkel, L. (2006). Extremely randomized trees. Mach. Learn. *63*, 3–42. https://doi.org/10.1007/s10994-006-6226-1.

51. Lopez, K., Fodeh, S.J., Allam, A., Brandt, C.A., and Krauthammer, M. (2020). Reducing Annotation Burden Through Multimodal Learning. Front. Big Data *3*, 19. https://doi.org/10.3389/fdata.2020.00019.

52. Bray, S.M., Mulle, J.G., Dodd, A.F., Pulver, A.E., Wooding, S., and Warren, S.T. (2010). Signatures of founder effects, admixture, and selection in the Ashkenazi Jewish population. Proc. Natl. Acad. Sci. USA *107*, 16222–16227. https://doi.org/10.1073/pnas.1004381107.

53. Joseph, T., Auger, S.D., Peress, L., Rack, D., Cuzick, J., Giovannoni, G., Lees, A., Schrag, A.E., and Noyce, A.J. (2019). Screening performance of abbreviated versions of the UPSIT smell test. J. Neurol. *266*, 1897–1906. https://doi.org/10.1007/s00415-019-09340-x.